Inorganic Chemistry
Article
pubs.acs.org/IC

Structures and Physical Properties of Layered Oxyselenides $Ba_2MO_2Ag_2Se_2$ (M = Co, Mn)

Tingting Zhou,[†,‡] Yumei Wang,[‡] Shifeng Jin,*[,†,‡] Dandan Li,[†,‡] Xiaofang Lai,[†,‡] Tianping Ying,[†,‡] Han Zhang,[†,‡] Shijie Shen,[†,‡] Wenjun Wang,[†,‡] and Xiaolong Chen*[,†,‡,§]

[†]Research & Development Center for Functional Crystals and [‡]Laboratory for Advanced Materials & Structure Analysis, Beijing National Laboratory for Condensed Matter Physics, Institute of Physics, Chinese Academy of Sciences, Beijing 100190, China
[§]Collaborative Innovation Center of Quantum Matter, Beijing, China

S *Supporting Information*

ABSTRACT: Two new layered oxyselenides, $Ba_2MO_2Ag_2Se_2$ (M = Co, Mn), have been successfully synthesized via solid-state reaction. It is found that these two compounds, consisting of the infinite MO_2 square planes and antifluorite-type Ag_2Se_2 layers separated by barium, possess new structural features while keeping *I*4/*mmm* symmetry. A detailed calculation on the discrete coordination of transition metals by oxygen in the two compounds and $Ba_2ZnO_2Ag_2Se_2$ revealed quite different energy landscapes. The calculated results indicate that the manganese compound favors adoption of the *I*4/*mmm* space group, while the cobalt compound could be at the boundary of the transition between the *I*4/*mmm* and *Cmca* phases. In $Ba_2CoO_2Ag_2Se_2$, the coexistence of a large barium ion and a Ag_2Se_2 layer expands the oxide layer significantly and results in the largest Co−O bond length in the square-planar sheet ever reported. $Ba_2CoO_2Ag_2Se_2$ is near-stoichiometric, whereas $Ba_2MnO_2Ag_2Se_2$ contains 7% silver vacancies, which is explained by the mixed valence of the manganese ion between 2+ and 3+. In $Ba_2CoO_2Ag_2Se_2$, the zero-field-cooled and field-cooled susceptibilities bifurcate at 159 K, located between two antiferromagnetic (AFM) transitions. Meanwhile, $Ba_2MnO_2Ag_2Se_2$ shows high-temperature Curie−Weiss behavior, followed by a low-temperature AFM transition with T_N = 32 K. They both exhibit semiconducting behavior with resisitivities of about $10^5 \Omega$ cm at room temperature. The optical band gaps are determined to be 1.49 and 1.18 eV for $Ba_2CoO_2Ag_2Se_2$ and $Ba_2MnO_2Ag_2Se_2$, respectively. Band structure calculations reveal that $Ba_2CoO_2Ag_2Se_2$ is a direct-gap semiconductor, with a calculated band gap of 1.147 eV; however, $Ba_2MnO_2Ag_2Se_2$ failed to reproduce the semiconducting behavior within an A-type AFM model.

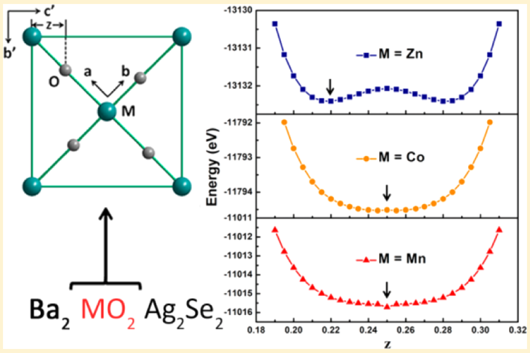

INTRODUCTION

Low-dimensional magnetic systems have been a major subject of theoretical and experimental studies because of their special physical properties and potential applications in areas as diverse as high-temperature superconductivity and colossal magnetoresistance.[1,2] The recent discovery of superconductivity in layered iron chalcogenides[3] has evoked a renewed interest in low-dimensional 3d transition-metal chalcogenides, where a majority of lately discovered systems are oxychalcogenides.

Because of the different sizes and coordination requirements of oxygen and heavier chalcogen anions, oxychalcogenides tend to adopt structures with distinct oxide and chalcogenide layers. For example, LnM′OCh (Ln = rare earth, Bi; M′ = Cu, Ag; Ch = S, Se, Te) consists of alternating $(Ln_2O_2)^{2+}$ fluorite layers and $(M'_2Ch_2)^{2-}$ antifluorite layers.[4−6] Meanwhile, more frequently the transition metal M can be found bonding within the oxide layers. In the oxysulfides $A_2MO_2Cu_2S_2$ (where A is an alkaline-earth metal and M is a transition metal), the more polarizable sulfur anion bonds to copper in $(Cu_2S_2)^{2-}$ antifluorite-type layers, and the less polarizable oxygen anion bonds to the divalent M^{2+} ions in square-planar $(MO_2)^{2-}$ layers.[7,8] Related oxychalcogenides still include compounds containing antitype planar M_2O layers with M two-coordinated by oxygen ions and four-coordinated by chalcogen ions, such as $La_2Fe_2Se_2O_3$ and the recently reported $Na_2Fe_2Se_2O$.[9,10]

Among layered oxychalcogenides, the $A_2MO_2M'_2Ch_2$ series in the $Sr_2Mn_3Sb_2O_2$[11] structure type (space group *I*4/*mmm*) have been extensively investigated and attracted much interest because of their novel magnetic and electronic properties. These compounds offer high-symmetry structures with transition-metal ions in strictly planar oxide layers, irrespective of the nature of the alkaline-earth cation or the chalcogen anion, and may be good model compounds that will contribute to the development of theories of low-dimensional solids. For example, $(Sr_{1-x}Ba_x)_2CoO_2Cu_2S_2$ are the rare examples of systems with high-spin cobalt ions in a coordination environment that is a highly distorted CoO_4S_2 octahedron.[12] Meanwhile, in $Sr_2MnO_2Cu_{1.5}(S_{1-x}Se_x)_2$, the CE-type magnetic structure is adopted by the sulfide end member (x = 0). With

Received: January 26, 2014
Published: April 4, 2014

dx.doi.org/10.1021/ic500203k | *Inorg. Chem.* 2014, 53, 4154−4160

an increase of the selenium content, an A-type magnetic structure develops and coexists with the CE-type phase until $x \sim 0.15$, and for $x \geq 0.0175$, the A-type structure accounts for all of the magnetic scattering.[13]

In tetragonal $A_2MO_2M'_2Ch_2$, the M−O bond length is equal to half of the lattice constant a and the incorporation of large atoms inevitably increases the length of this bond. In the extreme case, $Ba_2ZnO_2Ag_2Se_2$, when the ZnO_2 plane is placed under tension to accommodate the large Ba^{2+}, Ag^{+}, and Se^{2-} ions, the square-planar coordination of zinc by oxygen is unsustainable and fragments into discrete $[ZnO_2]^{2-}$ linear anionic units, and the symmetry is reduced from tetragonal *I*4/*mmm* to orthorhombic *Cmca*.[14] It will be an interesting issue to investigate the magnetic coupling between the rarely known linear anionic units. However, zinc is nonmagnetic, and there will be no magnetic coupling in the zinc case. In this work, the nonmagnetic zinc atom in the orthorhombic phase was entirely replaced by magnetic cobalt and manganese atoms, and the substitution successfully leads to two new compounds, $Ba_2MO_2Ag_2Se_2$ (M = Co, Mn). Interestingly, a mass of transmission electron microscopy (TEM) observations and X-ray diffraction (XRD) studies revealed that, although the crystal lattices have been enormously expanded as in the zinc phase, the two title compounds both keep the infinite MO_2 square planes and *I*4/*mmm* symmetry. A detailed calculation on the discrete coordination of transition metals by oxygen in the three compounds revealed quite different energy landscapes, the result of which is well confirmed by our experimental observations. The magnetic, electronic-transport, and optical properties and structural variation tendency of these compounds are also investigated.

EXPERIMENTAL SECTION

Synthesis of $Ba_2MO_2Ag_2Se_2$ (M = Co, Mn). $Ba_2MO_2Ag_2Se_2$ (M = Co, Mn) polycrystalline samples were synthesized by reacting stoichiometric amounts of BaO, Co/Mn, Ag, and Se. Because of the air sensitivity of BaO, manipulations of the reactants prior to synthesis were performed in an argon-filled glovebox. The reactants were intimately mixed thoroughly using an agate pestle and mortar and pressed into 10-mm-diameter pellets at 20 MPa. The pellets were placed in dry alumina crucibles inside silica tubes. The tubes were sealed under a vacuum (10^{-4} Pa) and heated in a muffle furnace. The pellets were heated at 400 °C for 15 h to ensure reaction of selenium with the element metals prior to heating at a synthesis temperature of 850 °C for 24 h, followed by cooling at the natural rate of the furnace.

Crystal Structure Determinations. Powder XRD was performed at room temperature using a Panalytical diffractometer (X'Pert PRO MRD) operating in Bragg−Brentano geometry with Cu Kα radiation and a graphite monochromator. Phase characterizations were realized from powder XRD patterns using the PDF2-2010 database. Indexing of the compounds was realized using the *DICVOL91* program.[15] Rietveld refinement was performed using the *FULLPROF* program.[16]

TEM. Electron diffraction (ED) patterns were taken on a JEOL-2010 transmission electron microscope. The specimens for electron microscope observations were prepared by dispersing the powders in ethanol and depositing a drop of this solution on a holey carbon grid.

X-ray Photoelectron Spectroscopy (XPS). The XPS data were taken on an AXIS-Ultra instrument from Kratos using monochromatic Al Kα radiation (225 W, 15 mA, and 15 kV) and low-energy electron flooding for charge compensation. To compensate for surface charge effects, binding energies were calibrated using the C 1s hydrocarbon peak at 284.80 eV.

Magnetic Susceptibility Measurements. Measurements of the direct-current magnetic susceptibility were conducted on Quantum Design PPMS magnetometers in the temperature range 10−300 K and at magnetic fields of 0.1 or 1 T. Approximately 10−20 mg of material was weighed accurately into a gelatin capsule. Measurements of the susceptibility were made upon warming in a field of 0.1 or 1 T, first after cooling in zero field (ZFC) and then again after cooling in the measuring field (FC).

Transport Measurements. The resistivity was measured in a Quantum Design PPMS using the standard four-probe configuration. The sample pellets were cut into bars, and four fine platinum wires were attached on the bar with silver paste.

Diffuse-Reflectance Spectroscopy. A Cary model 5000 ultraviolet−visible light−near-infrared (UV−vis−NIR) spectrophotometer with a diffuse-reflectance accessory was used to measure the spectrum of samples over the range 240−2600 nm. $BaSO_4$ was used as a reference material. Reflectance spectra were converted to absorbance using the Kubelka−Munk function.[17,18]

First-Principles Calculations. The first-principles calculations for $Ba_2MO_2Ag_2Se_2$ (M = Zn, Co, Mn) were based on density functional theory under the generalized gradient approximation with Perdew−Burke−Ernzerhof[19] for the exchange-correlation potentials. All calculations were performed using the Cambridge Serial Total Energy Package.[20] The ultrasoft pseudopotentials[21] were used to model the electron−ion interactions. The experimental crystallographic parameters were adopted in our calculations (crystallographic parameters for $Ba_2ZnO_2Ag_2Se_2$ are from ref 14). A kinetic energy cutoff of 380 eV and Monkhorst−Pack *k*-point meshes with a span of 0.04/Å^3 in the Brillouin zone were chosen. The total energy calculation was performed under spin-unpolarized conditions. A series of total energies of $Ba_2MO_2Ag_2Se_2$ (M = Zn, Co, Mn) were obtained by altering the positions of the oxygen ions along the nearest M−M direction with other experimental crystallographic parameters fixed. As for the electronic structure calculation, the adopted density functional is the local-spin density approximation plus on-site Coulomb interaction U (LSDA+U) with U values of 5 eV for both the cobalt and manganese ions. We considered a probable antiferromagnetic (AFM) lattice for the cobalt spins, where the nearest-neighbor moments within the CoO_2 planes couple antiferromagnetically and the spins in next-nearest-neighbor layers are aligned parallel.[12] In $Ba_2MnO_2Ag_2Se_2$, an A-type AFM structure for manganese ions and a virtual crystal approximation for silver occupation were adopted.[13]

RESULTS AND DISCUSSION

Crystal Structures and Compositions. Figure 1 shows the powder XRD patterns of $Ba_2CoO_2Ag_2Se_2$ and $Ba_2MnO_2Ag_2Se_2$. All of the reflections in $Ba_2CoO_2Ag_2Se_2$ can be indexed with a tetragonal or orthorhombic unit cell, with no peaks due to impurity being present. However, our attempts to obtain $Ba_2MnO_2Ag_2Se_2$ in a pure form with a high-temperature synthesis route always revealed that the samples contain trace quantities of impurities, such as Ag and BaSe. Moreover, a multiple-phase Rietveld refinement of $Ba_2MnO_2Ag_2Se_2$ revealed 7.3(3)% silver deficiencies. Considering that most of the reported manganese oxychalogenides contain 25% silver or copper deficiencies,[22] a variety of samples with nominal compositions $Ba_2MnO_2Ag_{2-x}Se_2$ ($0 \leq x \leq 0.5$, including the refined composition) and different synthesis temperatures between 1073 and 1173 K have been tried but failed to improve the purity of the target compound. Structural and physical characterizations were based on samples synthesized with a nominal composition $Ba_2MnO_2Ag_2Se_2$. As reported in $Ba_2ZnO_2Ag_2Se_2$, it is hard to distinguish orthorhombic *Cmca* and tetragonal *I*4/*mmm* from XRD patterns because the difference is quite subtle in powder XRD patterns.[14] However, TEM is a more useful tool for charactering the crystal symmetry because the information on systematic absences could be fully explored by the two-dimensional ED patterns from polycrystalline crystals with various orientations. The crystallographic information such as lattice parameters, crystal

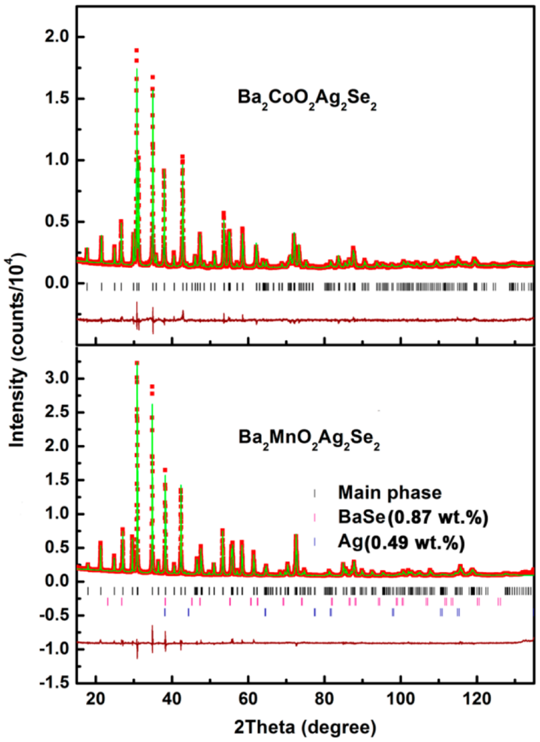

Figure 1. Rietveld refinement against powder XRD data for the samples of $Ba_2CoO_2Ag_2Se_2$ (upper) and $Ba_2MnO_2Ag_2Se_2$ (below). The red solid squares stand for experimental data, the green solid lines for calculated results, and the wine solid lines at the bottom for the difference. The vertical bars indicate reflection positions.

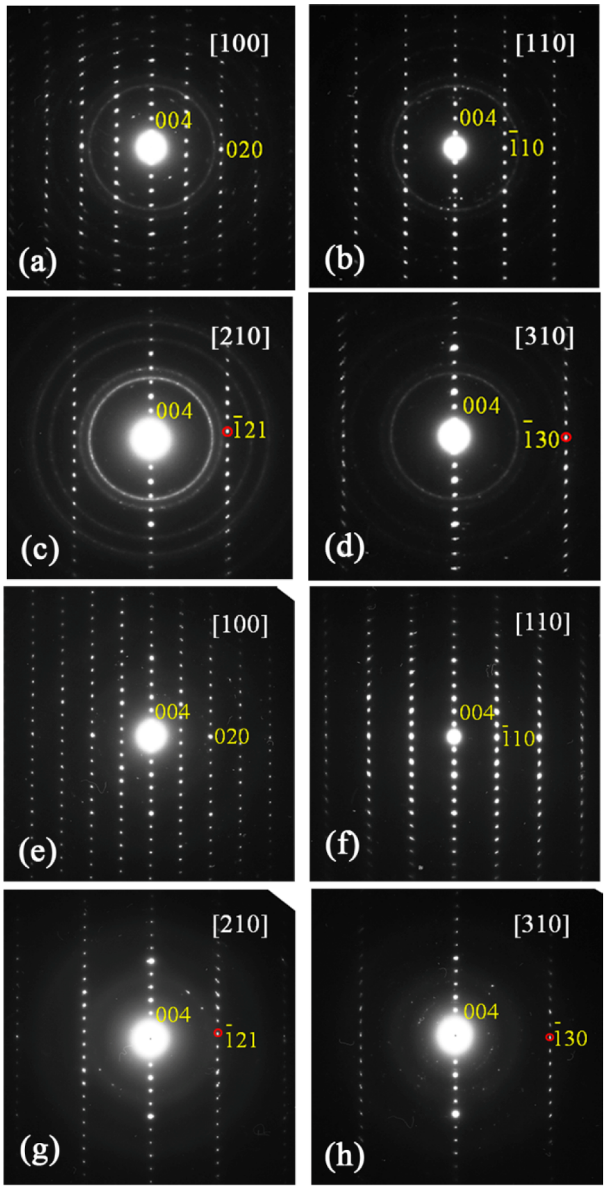

Figure 2. ED patterns for various zones indexed on the *I*4/*mmm* cell for $Ba_2CoO_2Ag_2Se_2$ (a–d) and $Ba_2MnO_2Ag_2Se_2$ (e–h).

symmetry, and orientation can be easily obtained from the ED patterns. Figure 2 shows the ED patterns for the $Ba_2CoO_2Ag_2Se_2$ and $Ba_2MnO_2Ag_2Se_2$ specimens. The diffraction rings appearing in Figure 2a–d come from the thin golden foil evaporated onto the holey carbon film, which was used to calibrate the ED camera length. All of the spots in the patterns can be successfully indexed according to an ideal *I*4/*mmm* structure. It is found that there are no extra spots in the ED patterns with a mass of TEM observations. That is, the structure variations, including the change from tetragonal to orthorhombic with unit cell $c \times \sqrt{2}a \times \sqrt{2}a$ as reported previously in $Ba_2ZnO_2Ag_2Se_2$,[14] do not appear, and the symmetry of the examined $Ba_2MO_2Ag_2Se_2$ (M = Co, Mn) is *I*4/*mmm*.

Therefore, we performed the Rietveld refinement by adopting $Sr_2Mn_3Sb_2O_2$[11] as an initial structural model against the room-temperature data on the samples. The results are summarized in Tables 1 and 2, and the structure is shown in Figure 3. In $Ba_2CoO_2Ag_2Se_2$, the structure is built up by stacking infinite CoO_2 planar sheets and antifluorite-type Ag_2Se_2 layers alternatively along the *c* axis separated by barium ions. The sample is very close to stoichiometric in silver, with a refined composition of $Ba_2CoO_2Ag_{2.006(6)}Se_2$, similar to other oxychalcogenides containing cobalt ions.[12] It is worth noting that the occupancy of the silver atom exceeds unity, presumably because of the effect of correlations between the silver site occupancy and the displacement parameters, as reported in $(Sr_{1-x}Ba_x)_2CoO_2Cu_2S_2$.[12] The silver site occupancy of 1.003(3) could be considered to be unity within the statistical deviation.[23] The refined lattice parameters are a = 4.22323(7) Å and c = 20.0358(4) Å for the tetragonal cell, and the Co−O distance is equal to $a/2$ in the ideal structure. Table 3 lists the important bond lengths and angles obtained from the refinement. In order to accommodate the large Ba^{2+}, Ag^+, and Se^{2-} ions, the Co−O distance increases to 2.1116(1) Å from its already large value of 2.0490(1) Å in $Sr_2CoO_2Ag_2Se_2$,[24] considerably weakening the bonding between cobalt and oxygen atoms, and is close to 2.1424(2) Å in $Ba_2ZnO_2Ag_2Se_2$ in the *I*4/*mmm* model.[14] With four Co−O contacts of 2.1116(1) Å and two Co−Se contacts of 3.2566(14) Å, Co^{2+} is extremely underbonded in the bond valence sum (BVS) model (BVS of 1.287),[16] similar to the Zn^{2+} atoms in the zinc compound (BVS of 1.35).[14] It is worth noticing that $Ba_2CoO_2Ag_2Se_2$ presents the largest CoO_2 square plane ever reported. The seriously expanded oxide layers may have a great influence on the magnetic interaction. Following the relationship between the magnetic moment and coordination geometry of the Co^{2+} ion mentioned in ref 12, the magnetic moment of Co^{2+} here is estimated to be 3.7 μ_B. Meanwhile, the Ag−Se length of 2.7440(9) Å in $Ba_2CoO_2Ag_2Se_2$ is slightly less than

Table 1. Structural Results and Rietveld Refinements for $Ba_2MO_2Ag_2Se_2$ (M = Co, Mn) at Room Temperature

	$Ba_2CoO_2Ag_2Se_2$	$Ba_2MnO_2Ag_2Se_2$
mol wt	739.242	719.51
lattice	tetragonal	tetragonal
space group	*I*4/*mmm*	*I*4/*mmm*
a (Å)	4.22323(7)	4.26514(5)
c (Å)	20.0358(4)	19.7184(2)
V (Å^3)	357.353(11)	358.706(9)
Z	2	2
T (K)	298(2)	298(2)
D_x (g cm^{-3})	6.87	6.66
radiation type	Cu Kα	Cu Kα
wavelength (Å)	1.5418	1.5418
collection range 2θ (deg)	10−135	10−135
step size 2θ (deg)	0.017	0.017
R_p (%)	2.68	3.56
R_{wp} (%)	3.47	4.52
χ^2	2.01	2.98

Table 2. Fractional Atomic Coordinates and Equivalent Isotropic Displacement Parameters for $Ba_2CoO_2Ag_2Se_2$ (I) and $Ba_2MnO_2Ag_2Se_2$ (II)

	atom	*x*	*y*	*z*	U_{iso} (Å^2)	occupancy
I	Ba	0	0	0.41181(5)	0.0177(4)	1.0
	Co	0	0	0	0.0207(12)	1.0
	O	0	$^{1}/_{2}$	0	0.022(3)	1.0
	Ag	0	$^{1}/_{2}$	$^{1}/_{4}$	0.0306(6)	1.003(3)
	Se	0	0	0.16254(7)	0.0200(7)	1.0
II	Ba	0	0	0.41053(4)	0.0043(3)	1.0
	Mn	0	0	0	0.0210(11)	1.0
	O	0	$^{1}/_{2}$	0	0.017(3)	1.0
	Ag	0	$^{1}/_{2}$	$^{1}/_{4}$	0.0174(5)	0.927(3)
	Se	0	0	0.16134(6)	0.0075(5)	1.0

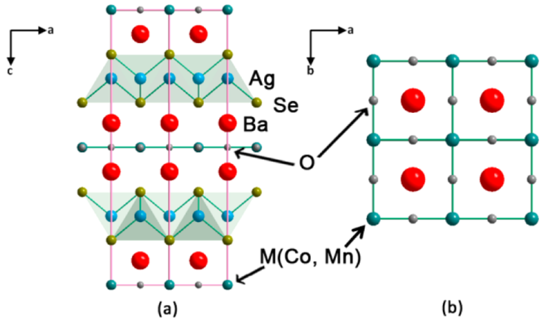

Figure 3. (a) Structure of $Ba_2MO_2Ag_2Se_2$ (M = Co, Mn) showing alternative stacking of MO_2 (M = Co, Mn) and Ag_2Se_2 layers (shaded parts). (b) Structural units of Ba_2MO_2 layers. The red large solid circles are barium atoms.

the value of 2.7647(14) Å in $Sr_2CoO_2Ag_2Se_2$.[24] The Ag_2Se_2 layer responds to expansion by a squashing of $AgSe_4$ tetrahedra in the *c* direction in $Ba_2CoO_2Ag_2Se_2$, reaching a less deformed tetrahedron.

Meanwhile, as shown in Table 2, the fractional occupancy of silver in $Ba_2MnO_2Ag_2Se_2$ is determined to be 92.7(3)% through a multiple-phase Rietveld refinement (Figure 1), close to that of $Ba_2MnO_2Ag_{1.854(6)}Se_2$, and we cannot rule out a small phase width. The quantitative refinement analysis revealed that, apart from the main phase, BaSe accounts for 0.87 wt % (2.7 mol %) and elemental Ag for 0.49 wt % (3.1 mol %). Compared with the lattice constant *a* of 4.0882(1) Å for $Sr_2MnO_2Ag_{1.5}Se_2$, $Ba_2MnO_2Ag_2Se_2$ contains a much larger Mn−O bond length [the Mn−O distance is equal to half of *a*, 4.26514(5) Å].[24] At the same time, the lattice constant *c* increases from 19.1179(2) Å in $Sr_2MnO_2Ag_{1.5}Se_2$ to 19.7184(2) Å in $Ba_2MnO_2Ag_2Se_2$. The larger lattice parameters may cause a lower oxidation state, borne out in the later discussion. With four Mn−O contacts of 2.1326(1) Å and two Mn−Se contacts of 3.1814(12) Å, Mn^{2+} is less underbonded (BVS of 1.59)[16] in compared with the cobalt and zinc compounds. A less deformed silver−selenium tetrahedron is also obtained in $Ba_2MnO_2Ag_2Se_2$ compared with $Sr_2MnO_2Ag_{1.5}Se_2$.[24]

To elucidate the structural peculiarity of adopting a $Sr_2Mn_3Sb_2O_2$-type structure, we assess the stabilities of $Ba_2MO_2Ag_2Se_2$ (M = Zn, Co, Mn) with a series of hypothetical positions of oxygen ions along the nearest M−M direction within the *Cmca* model. A detailed calculation on the discrete coordination of transition metals by oxygen in the three compounds revealed quite different energy landscapes. As shown in Figure 4, the total energy calculation of $Ba_2ZnO_2Ag_2Se_2$ shows that it is energetically more favorable for the oxygen ion to be located at two sites of $z = 0.22$ or 0.28, where *z* stands for the fractional coordinate of oxygen ions along the *c*′ axis in the *Cmca* lattice. The calculated results are well consistent with the experimental values of $z = 0.2224(15)$ and 0.2776(15) for $Ba_2ZnO_2Ag_2Se_2$ in ref 14. In contrast, the lowest calculated total energy of $Ba_2MnO_2Ag_2Se_2$ is obtained when $z = 0.25$; i.e., the oxygen ion is located at the center of the two nearest M−M ions, forming tetragonal *I*4/*mmm*. That is to say, the *I*4/*mmm* space group is energetically more favored in $Ba_2MnO_2Ag_2Se_2$, the result of which is well confirmed by our experimental observations. Interestingly, in $Ba_2CoO_2Ag_2Se_2$, the lowest calculated total energies are located at $z = 0.245$ or 0.255, not exactly at $z = 0.25$. The results suggest that the cobalt compound could be at the boundary of the transition between the *I*4/*mmm* and *Cmca* phases. A natural hypothesis is the introduction of much larger ions (such as the total or partial substitution of Te^{2-} in the Ch^{2-} site) may realize the tension required to stabilize the linear discrete $[CoO_2]^{2-}$ anionic units in $A_2CoO_2Ag_2Ch_2$. Moreover, calculation results also proved

Table 3. Selected Bond Lengths (Å) and Bond Angles (deg) of $Ba_2CoO_2Ag_2Se_2$ and $Ba_2MnO_2Ag_2Se_2$ and Corresponding Literature Values of $Sr_2CoO_2Ag_2Se_2$ and $Sr_2MnO_2Ag_{1.5}Se_2$[24]

bond/angle	$Ba_2CoO_2Ag_2Se_2$	$Ba_2MnO_2Ag_2Se_2$	$Sr_2CoO_2Ag_2Se_2$	$Sr_2MnO_2Ag_{1.5}Se_2$
Ag−Se (Å)	2.7440(9) × 4	2.7576(8) × 4	2.7647(14) × 4	2.7376(9) × 4
Co/Mn−O (Å)	2.1116(1) × 4	2.1326(1) × 4	2.0490(1) × 4	2.0441(1) × 4
Ba/Sr−O (Å)	2.7534(6) × 4	2.7677(5) × 4	2.6129(12) × 4	2.6654(7) × 4
Co/Mn−Se (Å)	3.2566(14) × 2	3.1814(12) × 2	3.002(2) × 2	2.9585(13) × 2
Se−Ag−Se (deg)	114.07(2) × 4	113.70(1) × 4	116.79(3) × 4	116.26(2) × 4
	100.63(3) × 2	101.31(3) × 2	95.66(5) × 2	96.61(3) × 2

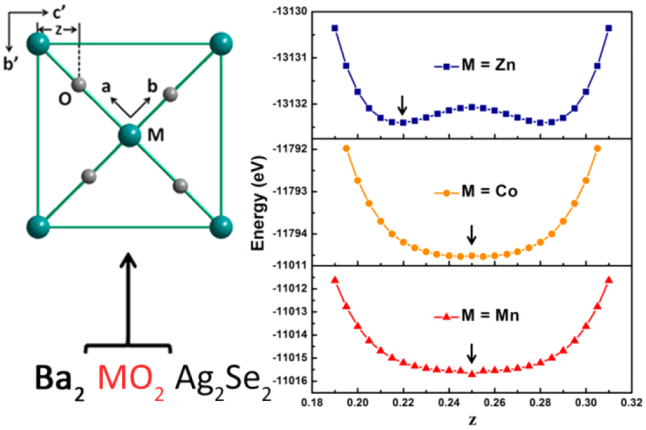

Figure 4. Total energies of $Ba_2MO_2Ag_2Se_2$ (M = Zn, Co, Mn) with a series of hypothetical positions of oxygen ions along the nearest M−M direction (*a* and *b* stand for crystal orientations in the *I*4/*mmm* space group, *b*′ and *c*′ stand for crystal orientations in the corresponding *Cmca* space group with unit cell $c \times \sqrt{2}a \times \sqrt{2}a$, *z* stands for the fractional coordinate of oxygen ions along the *c*′ axis, and the arrows in the right figure point to the *z* values from the experiment).

that the adoption of a linear coordination for Zn^{2+} in $Ba_2ZnO_2Ag_2Se_2$ is due to a lack of alternative products of lower energy to be realized in practice.

Magnetic Property. To investigate the influence of an enlarged perovskite-type A_2MO_2 oxide layer on the magnetic properties, we performed measurements of the temperature-dependent susceptibility. As shown in Figure 5, the magnetic susceptibility of $Ba_2CoO_2Ag_2Se_2$ shows a broad transition at about 220 K, suggesting low-dimensional AFM ordering of Co^{2+} ions. A second sharper feature was observed at about 144 K. The two successive transitions are similar to that of $Sr_2CoO_2Ag_2Se_2$, but the transition temperatures were shifted from 210 and 70 K to 220 and 144 K, respectively.[24] Similar behavior was also observed in La_2CoO_4.[25] Interestingly, at an intermediate temperature (159 K) between the two AFM transitions, the ZFC and FC curves bifurcate (defined as T_{bi}), which usually takes place at lower temperature.[8,12,24] The FC data show an increase, in contrast to a decrease in the ZFC data, upon cooling, suggesting the presence of a ferromagnetic contribution to the susceptibility. As shown in Figure S1 in the Supporting Information (SI), the bifurcation temperatures in oxyselenides seem to increase monotonically with expansion of the CoO_2 layers. The exact relationship needs further study. The Curie−Weiss-like upturn at low temperatures is presumably due to the paramagnetic impurities. The magnetic susceptibility of $Ba_2MnO_2Ag_2Se_2$ shows an AFM transition with $T_N \approx 32$ K, lower than the 67 K value of $Sr_2MnO_2Ag_{1.5}Se_2$. Fitting the data from 150 to 300 K to a Curie−Weiss law gives an effective moment of $\mu_{eff} = 5.3\ \mu_B$ and a Curie−Weiss temperature of 44.5 K. The effective magnetic moment is lower than the spin-only μ_{eff} of 5.92 μ_B expected for the high-spin d^5 configuration of Mn^{2+} but comparable to the value of 5.43 μ_B expected for a mean manganese oxidation state of 2.5+, considering that the moment derived from the Curie−Weiss formula is smaller than the spin state of the free ions. The positive Curie−Weiss temperature for $Ba_2MnO_2Ag_2Se_2$ (+44.5 K) suggest that the dominant exchange interactions in the temperature range 150−300 K are ferromagnetic.

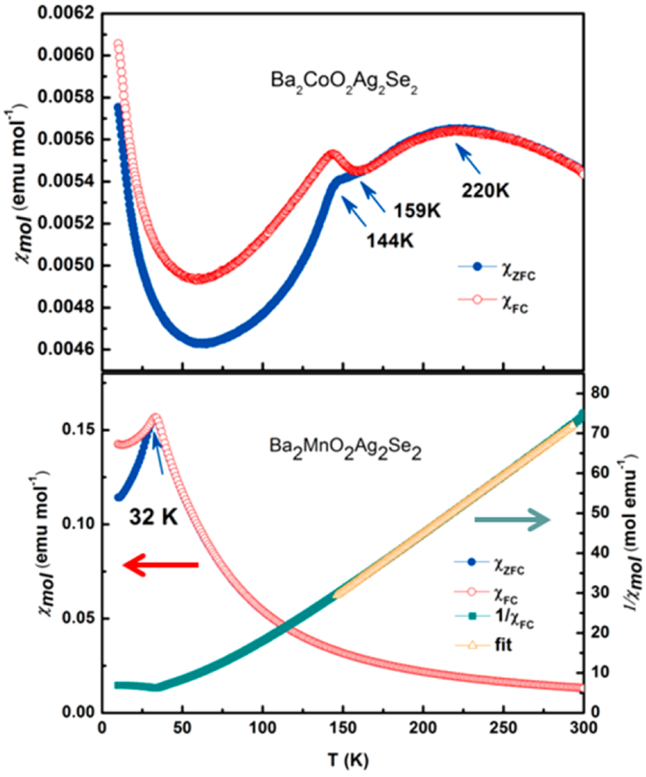

Figure 5. ZFC and FC magnetic susceptibilities for $Ba_2CoO_2Ag_2Se_2$ measured at 1 T (upper) and $Ba_2MnO_2Ag_2Se_2$ measured at 0.1 T (below). The linear fit to the Curie−Weiss law is shown as a yellow line (below).

Manganese Oxidation State. Because of the less electronegative properties of chalcogen atoms, lower transition-metal oxidation states may be stabilized in the oxychalcogenides than the one commonly found in perovskite-type oxide. For example, in the $Sr_2MnO_2Cu_{2m-\delta}S_{m+1}$ series (*m* = 1−3 and the intergrowth of the *m* = 1 and 2 members, which has an effective *m* of 1.5, $\delta \approx 0.5$), the manganese is oxidized to approximately the 2.5+ oxidation state,[22] lower than the usual oxidation states of 3+ and 4+ in perovskite-type oxide. Therefore, the system provided an ideal stage to investigate manganese with a low oxidation state in strictly planar oxide layers. The appearance of silver deficiency in the refined composition $Ba_2MnO_2Ag_{1.856(6)}Se_2$ implied that the Mn^{2+} ion is partial oxidized. In order to directly study the valence of the manganese ion, we carried out XPS. As shown in Figure 6, the Mn $2p_{3/2}$ photopeak binding energy maxima for this compound is 641.1 eV, located between the binding energies of Mn^{2+} and Mn^{3+} ions in MnO (640.4 eV) and Mn_2O_3 (641.9 eV).[26] This result indicated that the valence of manganese in $Ba_2MnO_2Ag_2Se_2$ is intermediate between 2+ and 3+, which explained the existence of silver vacancies.

Transport Property. The temperature-dependent electrical resistivities of $Ba_2CoO_2Ag_2Se_2$ and $Ba_2MnO_2Ag_2Se_2$ are presented in Figure 7. They both exhibit semiconducting behavior. The resistivities of as-prepared samples increase rapidly upon cooling from room-temperature values of 2.14×10^5 Ω cm for $Ba_2CoO_2Ag_2Se_2$ and 1.03×10^5 Ω cm for $Ba_2MnO_2Ag_2Se_2$. The values are several orders higher than that of their strontium counterparts,[24] consistent with the behavior in $(Sr/Ba)_2CoO_2Cu_2S_2$.[8] Using the thermal activation model $\rho_{ab}(T) = \rho_0 e^{E_a/k_BT}$ (ρ_0 is a prefactor, E_a the thermal activation energy, and k_B Boltzmann's constant) to fit the $\rho(T)$ data of $Ba_2MnO_2Ag_2Se_2$, we obtained $E_a = 0.22$ eV. For the cobalt

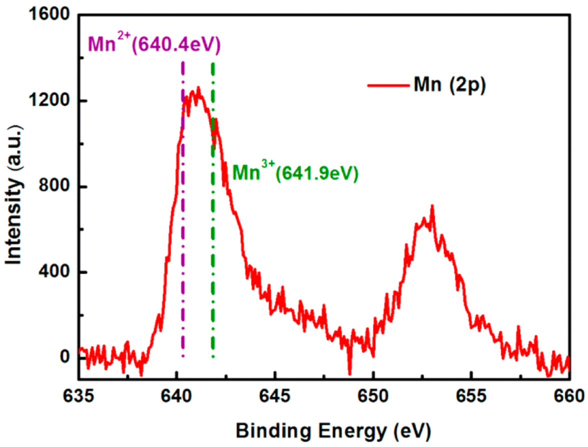

Figure 6. XPS Mn 2p signals of compound $Ba_2MnO_2Ag_2Se_2$ after background subtraction.

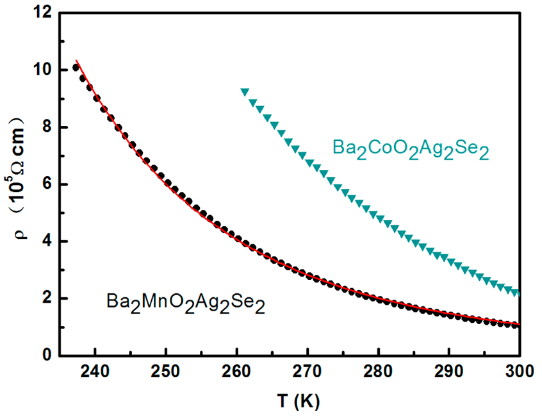

Figure 7. Electrical resistivity as a function of the temperature for the samples of $Ba_2CoO_2Ag_2Se_2$ and $Ba_2MnO_2Ag_2Se_2$. The red line is the fitting curve using the thermal activation model for $\rho(T)$.

compounds, the $\rho(T)$ data could not be fitted well using the thermal activation model.

Optical Band Gaps. The UV−vis−NIR diffuse-reflectance spectra of $Ba_2MO_2Ag_2Se_2$ (M = Co, Mn) in the region 500−2000 nm are displayed in Figure 8. In the $F(R)$ versus λ plots, the absorption edge can be deduced via the straightforward extrapolation method, and the optical band gap was calculated directly by converting the edge into energy units. The optical band gaps can be estimated as 1.49 and 1.18 eV for $Ba_2CoO_2Ag_2Se_2$ and $Ba_2MnO_2Ag_2Se_2$, respectively, and are consistent with the chestnut and gray-black colors of the material. The optical band gaps of the title compounds are much larger than the value of 0.064 eV for $Sr_2CoO_2Ag_2Se_2$ but less than the typical band gaps 2−3 eV of quaternary oxyselenides.[24,27] Note that the activation energy E_a extracted from the resistivity measurement on polycrystalline samples may be the energy gap between the donor or acceptor energy levels and a conduction or valence band. It is worth noting that, besides the absorption edge, there is another broad absorption peak at 1750 nm in the curve of $Ba_2CoO_2Ag_2Se_2$. According to the splitting energies of the d orbitals obtained for $(Sr_{1-x}Ba_x)_2CoO_2Cu_2S_2$,[12] which has a ligand field similar to that of $Ba_2CoO_2Ag_2Se_2$, this absorption peak could be caused by d−d transitions related to the cobalt ion.

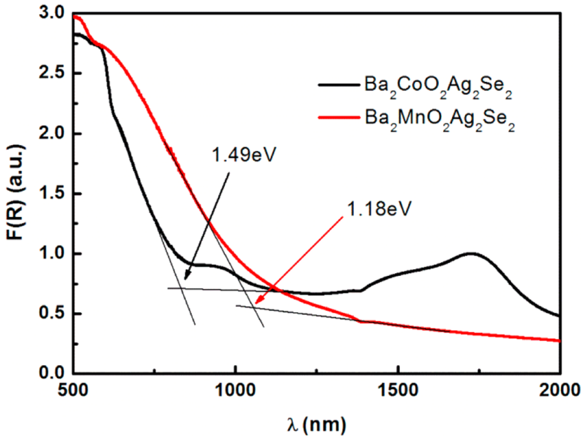

Figure 8. UV−vis−NIR diffuse-reflectance spectra of $Ba_2CoO_2Ag_2Se_2$ and $Ba_2MnO_2Ag_2Se_2$.

Electronic Structure Calculations. To gain insight into the electronic structures of $Ba_2MO_2Ag_2Se_2$ (M = Co, Mn), we performed first-principles band calculations by the spin-polarized LDA+U method. Figure 9a shows the energy-band structure of $Ba_2CoO_2Ag_2Se_2$ along the high-symmetry k lines. It is found that both the minimal-energy state in the conduction band and the maximal-energy state in the valence band are located at the Γ point ($k = 0$), indicating that $Ba_2CoO_2Ag_2Se_2$ is a direct-gap semiconductor. The calculated band gap of 1.147 eV is similar to the result of 1.49 eV determined by optical property measurement. The spin-polarized atom-resolved density of states are shown in Figure 9b. The maximum of the valence band is mostly occupied by the 4p orbitals of the selenium atoms and the 4d orbitals of the silver atoms, which are closely related to the transport and optical properties.

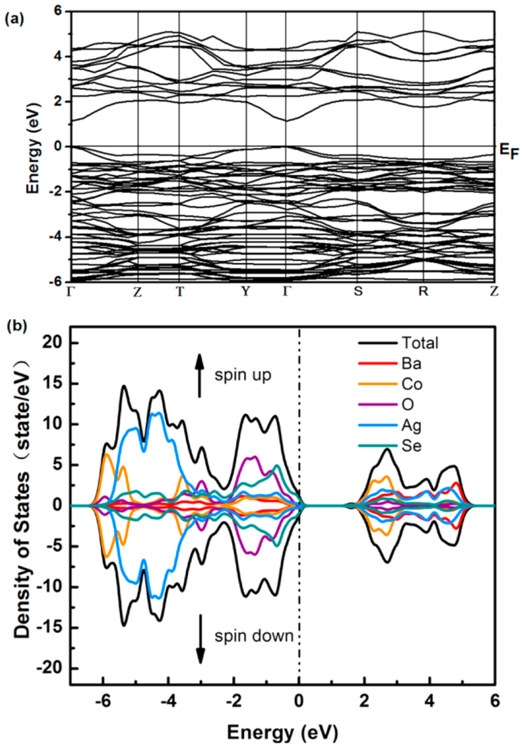

Figure 9. (a) Band structure of $Ba_2CoO_2Ag_2Se_2$. (b) Spin-polarized total and atom-resolved density of states of $Ba_2CoO_2Ag_2Se_2$.

Besides, we also carried out first-principles electronic structure calculations of $Ba_2MnO_2Ag_2Se_2$ with A-type AFM structure for manganese ions and virtual crystal approximation for silver occupation but failed to reproduce the semiconducting behavior (Figure S2 in the SI). The inconsistency may be due to the different spin ordering of manganese ions at low temperature.

■ CONCLUSION

In summary, we synthesized two new layered oxyselenides, $Ba_2MO_2Ag_2Se_2$ (M = Co, Mn). From a mass of TEM observations and powder XRD data, they are found to keep the infinite MO_2 square planes and crystallize in the $I4/mmm$ space group. A detailed calculation on the discrete coordination of transition metals by oxide in the three compounds revealed quite different energy landscapes. The calculated results indicate that the manganese compound favors the adoption of the $I4/mmm$ space group, while the cobalt compound could be at the boundary of the transition between the $I4/mmm$ and $Cmca$ phases. Moreover, the calculation results for $Ba_2ZnO_2Ag_2Se_2$ also proved that the adoption of the linear coordination for Zn^{2+} in $Ba_2ZnO_2Ag_2Se_2$ is due to a lack of alternative products of lower energy to be realized in practice. The coexistence of a large barium ion and a Ag_2Se_2 layer expands the oxide layer and results in a less deformed silver−selenium tetrahedron compared with their strontium analogues. Especially, $Ba_2CoO_2Ag_2Se_2$ contains the largest CoO_2 sheet ever reported, which may be related to the unusual magnetic behavior. $Ba_2CoO_2Ag_2Se_2$ is near-stoichiometric, whereas $Ba_2MnO_2Ag_2Se_2$ contains 7% silver vacancies, which is explained by the mixed valence of the manganese ion between 2+ and 3+. Meanwhile, the resistivities and the optical band gaps of the title compounds are greatly enhanced compared with their strontium analogues.[24] In addition, first-principles calculations confirm that $Ba_2CoO_2Ag_2Se_2$ is a semiconductor with a direct band gap of 1.147 eV located at the Γ point; however, $Ba_2MnO_2Ag_2Se_2$ failed to reproduce the semiconducting behavior within an A-type AFM model. Further neutron diffraction studies may shed light on the low-temperature AFM ordering behavior of this compound. Besides, the introduction of much larger ions (such as Te^{2-}) may realize the tension required to stabilize the linear discrete $[MO_2]^{2-}$ anionic units in $A_2MO_2M'_2Ch_2$ (M = Co, Mn).

■ ASSOCIATED CONTENT

Ⓢ Supporting Information

Listings of T_{bi} versus Co−O bond length in oxyselenides, first-principles calculation results for $Ba_2MnO_2Ag_2Se_2$, and X-ray crystallographic data in CIF format for $Ba_2MO_2Ag_2Se_2$ (M = Co, Mn). This material is available free of charge via the Internet at http://pubs.acs.org.

■ AUTHOR INFORMATION

Corresponding Authors

*E-mail: shifengjin@iphy.ac.cn. Tel: + 86 10 8264 9032. Fax: + 86 10 8264 9646.
*E-mail: chenx29@iphy.ac.cn. Tel: + 86 10 8264 9039. Fax: + 86 10 8264 9646.

Notes

The authors declare no competing financial interest.

■ ACKNOWLEDGMENTS

This work is supported by the National Natural Science Foundation of China (Grants 90922037, 51202286, 51072226, and 51102275) and the International Centre for Diffraction Data.

■ REFERENCES

(1) Bednorz, J. G.; Müller, K. A. *Z. Phys. B: Condens. Matter* **1986**, *64*, 189−193.
(2) von Helmolt, R.; Wecker, J.; Holzapfel, B.; Schultz, L.; Samwer, K. *Phys. Rev. Lett.* **1993**, *71*, 2331−2333.
(3) Hsu, F. C.; Luo, J. Y.; Yeh, K. W.; Chen, T. K.; Huang, T. W.; Wu, P. M.; Lee, Y. C.; Huang, Y. L.; Chu, Y. Y.; Yan, D. C.; Wu, M. K. *Proc. Natl. Acad. Sci. U.S.A.* **2008**, *105*, 14262−14264.
(4) Palazzi, M. *C. R. Seances Acad. Sci., Ser. 2* **1981**, *292*, 7899−7919.
(5) Palazzi, M.; Carcaly, C.; Flahaut, J. *J. Solid State Chem.* **1980**, *35*, 150−155.
(6) Kholodkovskaya, L. N.; Akselrud, L. G.; Kusainova, A. M.; Dolgikh, V. A.; Popovkin, B. A. *Mater. Sci. Forum* **1993**, *133−136*, 693−696.
(7) Zhu, W. J.; Hor, P. H. *J. Solid State Chem.* **1997**, *130*, 319−321.
(8) Zhu, W. J.; Hor, P. H.; Jacobson, A. J.; Crisci, G.; Albright, T. A.; Wang, S.-H.; Vogt, T. *J. Am. Chem. Soc.* **1997**, *119*, 12398−12399.
(9) Mayer, J. M.; Schneemeyer, L. F.; Siegrist, T.; Waszczak, J. V.; Van Dover, B. *Angew. Chem., Int. Ed. Engl.* **1992**, *31*, 1645−1647.
(10) He, J. B.; Wang, D. M.; Shi, H. L.; Yang, H. X.; Li, J. Q.; Chen, G. F. *Phys. Rev. B* **2011**, *84*, 205212(4).
(11) Brechtel, E.; Cordier, G.; Schaefer, H. *Z. Naturforsch., B: Anorg. Chem., Org. Chem.* **1979**, *34*, 777−780.
(12) Smura, C. F.; Parker, D. R.; Zbiri, M.; Johnson, M. R.; Gal, Z. A.; Clarke, S. J. *J. Am. Chem. Soc.* **2011**, *133*, 2691−2705.
(13) Adamson, P.; Hadermann, J.; Smura, C. F.; Rutt, O. J.; Hyett, G.; Free, D. G.; Clarke, S. J. *Chem. Mater.* **2012**, *24*, 2802−2816.
(14) Herkelrath, S. J. C.; Saratovsky, I.; Hadermann, J.; Clarke, S. J. *J. Am. Chem. Soc.* **2008**, *130*, 14426−14427.
(15) Boultif, A.; Louër, D. *J. Appl. Crystallogr.* **1991**, *24*, 987−993.
(16) Rodríguez-Carvajal, J. Satellite Meeting on Powder Diffraction of the XV Congress of the IUCr, Toulouse, France, 1990.
(17) Tauc, J. *Mater. Res. Bull.* **1970**, *5*, 721−729.
(18) Kubelka, P.; Munk, F. *Technol. Phys.* **1931**, *12*, 593−601.
(19) Perdew, J. P.; Burke, K.; Ernzerhof, M. *Phys. Rev. Lett.* **1996**, *77*, 3865−3868.
(20) Clark, S. J.; Segall, M. D.; Pickard, C. J.; Hasnip, P. J.; Probert, M. I. J.; Refson, K.; Payne, M. C. *Z. Kristallogr.* **2005**, *220*, 567−570.
(21) Vanderbilt, D. *Phys. Rev. B* **1990**, *41*, 7892−7895.
(22) Gál, Z. A.; Rutt, O. J.; Smura, C. F.; Overton, T. P.; Barrier, N.; Clarke, S. J.; Hadermann, J. *J. Am. Chem. Soc.* **2006**, *128*, 8530−8540.
(23) The CIF file provided for $Ba_2CoO_2Ag_2Se_2$ is the refinement result with silver site occupancy fixed as the integral.
(24) Jin, S. F.; Chen, X. L.; Guo, J. G.; Lei, M.; Lin, J. J.; Xi, J. G.; Wang, W. J.; Wang, W. Y. *Inorg. Chem.* **2012**, *51*, 10185−10192.
(25) Yamada, K.; Matsuda, M.; Endoh, Y.; Keimer, B.; Birgeneau, R. J.; Onodera, S.; Mizusaki, J.; Matsuura, T.; Shirane, G. *Phys. Rev. B* **1989**, *39*, 2336−2343.
(26) Oku, M.; Hirokawa, K.; Ikeda, S. *J. Electron Spectrosc. Relat. Phenom.* **1975**, *7*, 465−473.
(27) Clarke, S. J.; Adamson, P.; Herkelrath, S. J. C.; Rutt, O. J.; Parker, D. R.; Pitcher, M. J.; Smura, C. F. *Inorg. Chem.* **2008**, *47*, 8473−8486.